Robotica (2023), **41**, pp. 236–258
doi:10.1017/S0263574722001266

CAMBRIDGE UNIVERSITY PRESS

RESEARCH ARTICLE

Terminal sliding-mode disturbance observer-based finite-time adaptive-neural formation control of autonomous surface vessels under output constraints

Amir Naderolasli[1], Khoshnam Shojaei[1,2,*] and Abbas Chatraei[1,2]

[1]Department of Electrical Engineering, Najafabad Branch, Islamic Azad University, Najafabad, Iran and [2]Digital Processing and Machine Vision Research Center, Najafabad Branch, Islamic Azad University, Najafabad, Iran
*Corresponding author. E-mail: khoshnam.shojaee@gmail.com

Received: 31 March 2022; **Revised:** 5 July 2022; **Accepted:** 17 August 2022; **First published online:** 12 September 2022

Keywords: disturbance observer, dynamic surface control, finite-time, formation control, leader-follower, output constraints

Abstract

This paper proposes a tracking controller for the formation construction of multiple autonomous surface vessels (ASVs) in the presence of model uncertainties and external disturbances with output constraints. To design a formation control system, the leader-following strategy is adopted for each ASV. A symmetric barrier Lyapunov function (BLF), which advances to infinity when its arguments reach a finite limit, is applied to prevent the state variables from violating constraints. An adaptive-neural technique is employed to compensate uncertain parameters and unmodeled dynamics. To overcome the explosion of differentiation term problem, a first-order filter is proposed to realize the derivative of virtual variables in the dynamic surface control (DSC). To estimate the leader velocity in finite time, a high-gain observer is effectively employed. This approach is adopted to reveal all signals of the closed-loop system which are bounded, and the formation tracking errors are semi-globally finite-time uniformly bounded. The computer simulation results demonstrate the efficacy of this newly proposed formation controller for the autonomous surface vessels.

1. Introduction

Formation control has been a major research concern in recent years because of its practicability in persistent surveillance, target tracking, transportation,etc. The ability to coordinate multiple mobile robots in comparison with a single complex robot is not limited to performance, reliability, adaptability and flexibility [1]. The formation control challenges correspond to designing, stabilizing, path-following and tracking controllers to make a group of autonomous vehicles to hold or track the appropriate positions together with orientations as to one or more reference points. There exist many approaches in obtaining an appropriate formation which can be branched into leader-following approaches [2, 3], behavior-based techniques [4, 5] and virtual-structure methods [6, 7]. The leader-follower formation control is the preferred in practice because of its simplicity and reliability [8]. This issue has been addressed by considering many practical aspects for tractor trailers [9], car-like mobile robots [10] and underwater vehicles [11]. In ref. [12], a dynamic surface control (DSC) approach is proposed for autonomous surface vessel (ASVs) in the presence of uncertainties and ocean disturbances. To provide the transient performance specifications on the formation errors, the prescribed performance control (PPC) is applied to the control design [13]. Thus, a leader-following attitude control is proposed by ref. [14] for the spacecraft formation subjects to a preassigned performance, where unknown inertial parameters, external disturbance torques and unmodeled uncertainties are taken into account.

Managing the constraints in a rigorous manner of control design and analysis has become the focus in different fields of science and engineering, because of their theoretical challenges and essence in real-world applications [15]. In the physical systems, constraints are ubiquitous, manifesting themselves

as physical stoppages, saturation, performance and safety specifications. The constraints' violation in a process may lead to degradation in performance, accidents or system damage. The Barrier Lyapunov function (BLF)-based control design is applied for these challenges to assure the constraint states. In this context, the barrier function $\Upsilon(x)$ is proposed as continuous function where the value tends to be at infinity when x approaches to the feasible region boundary [16]. The model predictive control is assessed in ref. [17] for the formation control by introducing constraints in the cost function as coupling terms. To assess the line-of-sight (LOS) range and angle constraints, tan-type BLF are suggested in the control approach [18]. In ref. [19], an adaptive NN control with the asymmetric BLF is adopted in the formation control of marine vessels. Moreover, the finite-time is more advantages than the asymptotic control due to the protocols applied in its design by finite-time control, which are of rapid convergence rate [20, 21]. The minimal learning parameters (MLP) and NN approaches are applied to all ASVs through finite-time formation control in ref. [22]. The major features of finite-time control consist of high tracking precision, powerful disturbance rejection, appropriate robustness and fast convergence rate.

All ASVs are exposed to different types of marine disturbances like waves and ocean currents. Unexpected external disturbances have an inverse effects on the system performance to an extent that it may lead to the control system destabilization [23, 24]. Applying a nonlinear disturbance observer will be contributive in rejecting disturbances in all ASVs [25, 26]. These observers are devised for compensating the inflicted forces and the accelerations of the vessels. These disturbances are modeled through first- and second-order models in the control design in ref. [27]. To enhance the antidisturbance capability and improve the control accuracy of complex systems, various disturbance rejection methods have been extensively studied. Researchers in refs. [28, 29] devised a disturbance rejection based on terminal sliding-mode control. This newly finite-time control lacks the capability of disturbance rejection, which may lead to the performance degradation due to impact on the limited and predefined error bounds.

Motivated by the above discussions, the control objective is to make the constrained formation control of all ASVs moving on a specified trajectory in the presence of the imposed environment disturbances under output constraints without velocity measurements. Although the previous disturbance observers are able to provide the tracking controller design with a high-precision estimation of disturbances, nearly all of them are designed such that they only assure that the disturbance estimation errors converge to zero without finite settling time in the stability analysis. The infinite settling time is not desirable during the formation control problem execution. Moreover, if the imposed disturbances on the dynamics of all ASVs are not compensated within the finite-time, the improper transient performance of the formation errors causes collisions and will affect in the deterioration of control efficiency. However, the trajectory errors of all ASVs in the formation control problem are transgressed from the limited and predefined bounds due to the limited field-of-view (FOV). Consequently, to cope with these challenges, a BLF-based constrained control structure with a disturbance observer design is proposed for the formation control problem of ASVs that improve the transient performance. Both the controller and disturbance observer are designed through finite-time approach.

Compared with previous related works, the main contributions of this article are expressed as follows:

- For the first time, the finite-time BLF-based DSC approach is successfully combined with a finite-time terminal sliding-mode disturbance observer for the formation control of ASVs due to the powerful disturbance rejection of the finite-time technique which increases effectively the convergence rate of the system response and compensates the disturbance effects in finite-time.
- Compared with the available obtained results [30–33], the BLF-based control laws are proposed for all ASVs to solve the formation control problem while making them keep the formation tracking errors in the limited and predefined bounds in the presence of model uncertainties, external disturbances and output states constraints.
- Compared with [34–36], an effective nonlinear terminal sliding-mode disturbance observer is applied to compensate the imposed environment disturbance effects in the formation control of these systems. The proposed controller guarantees the asymptotic trajectory tracking and

https://doi.org/10.1017/S0263574722001266 Published online by Cambridge University Press

removes the restrictions of the previous methods that require the external disturbances to be constant or its first-time derivative to be bounded.

- The suggested control design is performed for the full constrained states and without the velocity measurements. Applying of a high-gain observer (HGO) is an effective technique in the design of the output feedback control for the formation control problem of ASVs, which does not require any prior knowledge of the system dynamic model.
- Compared with [37–40], in the distributed control, the communication strategy not only is achieved based on the graph theory but also in the formation control problem, this issue is achieved based on the image vision, which is affected under the limited FOV. To solve this problem, it is necessary to consider limited FOV constraints in the formation control problem which imposes some restrictions on the tracking errors.

The rest of this article is organized as follows. Preliminaries and problem statements are presented in Section 2. The BLF is introduced in Section 3. The formation controller design for all ASVs is implemented in Section 4. The simulation results are presented in Section 5, and the article is concluded in Section 6.

2. Preliminaries and problem statements

Consider a group of cooperative autonomous surface vessels governed by the following kinematic and dynamic equations:

$$\begin{aligned} \dot{\eta}_i &= J_i(\psi_i)\upsilon_i \quad i = 1, \ldots, N, \\ M_i\dot{\upsilon}_i + C_i(\upsilon_i)\upsilon_i + D_i(\upsilon_i)\upsilon_i + G_i(\eta_i) &= \tau_i + \tau_{di}. \end{aligned} \tag{1}$$

where $M_i > 0$ is the inertia matrix, $C_i(\upsilon_i)$ is the total Coriolis and Centripetal acceleration matrix, $D_i(\upsilon_i)$ is the damping matrix, the vector $\eta_i = [x_i, y_i, \psi_i]^T$ is the output of all ASVs, $\upsilon_i = [u_i, v_i, r_i]^T$ is the vector of angular velocity, $\tau_i \in R^3$ is the control inputs and the vector $\tau_{di} = [\tau_{d1}, \tau_{d2}, \tau_{d3}]^T \in R^3$ contains the external disturbances, and $G_i(\eta_i) \in R^3$ is the gravity vector. Moreover, the rotational matrix $J_i(\psi_i)$ and the dynamic equations of velocities are defined as follows:

$$J_i(\psi_i) = \begin{pmatrix} \cos\psi_i & -\sin\psi_i & 0 \\ \sin\psi_i & \cos\psi_i & 0 \\ 0 & 0 & 1 \end{pmatrix}, \tag{2}$$

$$\begin{cases} m_{11i}\dot{u}_i = m_{22i}v_i r_i - d_{11i}u_i + \tau_{ui} - \tau_{wui}(t), \\ m_{22i}\dot{v}_i = -m_{11i}u_i r_i - d_{22i}v_i - \tau_{wvi}(t), \\ m_{33i}\dot{r}_i = (m_{11i} - m_{22i})u_i v_i - d_{33i}r_i + \tau_{ri} - \tau_{wri}(t). \end{cases} \tag{3}$$

With respect to kinematics and dynamics of all ASVs, the state equations are expressed as:

$$\begin{cases} \dot{\eta}_i = J_i(\psi_i)\upsilon_i \\ \dot{\upsilon}_i = M_i^{-1}(\tau_i + \tau_{di} - C_i(\upsilon_i)\upsilon_i - D_i(\upsilon_i)\upsilon_i - G_i(\eta_i)) \,. \end{cases} \tag{4}$$

The solutions of formation control consist of position-based, distance-based, orientation-based and their combinations. In this article, the position-based formation control is applied to the autonomous surface vessels. The geometric structure of two autonomous surface vessels moving in a leader-follower formation is shown in Fig 1. The LOS range ρ_i and angle λ_i between the leader and the followers are

https://doi.org/10.1017/S0263574722001266 Published online by Cambridge University Press

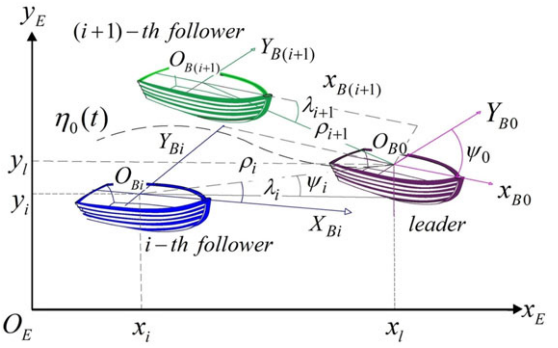

Figure 1. *A leader-follower formation structure.*

defined as:

$$\rho_i = \sqrt{(x_0 - x_i)^2 + (y_0 - y_i)^2},$$
$$\lambda_i = a\tan 2(y_0 - y_i, x_0 - x_i). \tag{5}$$

The objective is to design a control input τ_i for the follower i to track its leader with desired command where the following formation tracking errors are required to be constrained. In this context, let a desired reference trajectory $\eta_0 = [x_0, y_0, \psi_0]^T$ and its first-time derivatives $\dot{\eta}_0$ provide the leading formation problem, and then, the formation tracking errors are defined for each autonomous surface vessel as follows:

$$z_{1i}(t) = \eta_i(t) - \eta_0(t). \quad i = 1, \ldots, N. \tag{6}$$

The formation tracking errors for each autonomous surface vessel in the formation problem should meet the constraint requirements due to the limited FOV; thus, to assure the formation control objective, the following inequality must be of concern:

$$\|z_{1i}(t)\| < \beta_i \quad i = 1, \ldots, N. \tag{7}$$

where z_{1i} denotes the formation tracking error and β_i is the constrained bound of the tracking error for $i = 1, \ldots, N$.

Lemma 2.1. Young's inequality (ref. [27]) *For any* $\forall(x, y) \in \Re^2$, *the following inequality holds true:*

$$xy \leq \frac{\vartheta^p}{p}|x|^p + \frac{1}{q\vartheta^q}|y|^q, \tag{8}$$

where $\vartheta > 0$, $p > 1$, $q > 1$ *and* $(p-1)(q-1) = 1$.

Remark 1. A critical issue in the formation control problem is designing an appropriate algorithm to make the team of autonomous surface vessels to cover a desired formation. If the positions of individual autonomous surface vessels are controlled in an active sense, the autonomous surface vessels can move towards their desired positions any interact. Then, the surface vessels need to maintain their formation as a rigid body. Each autonomous surface vessel can only draw decisions based on the local information within a certain locality due to limited FOV, limited sensing range and communication constraints. In the available studies, the control problem in case of output constraints is not of concern. Moreover, there exist no strict theoretical basis to indicate that these constraints will never be violated. For safety and security, this issue cannot be ignored in practice. In this article, a symmetric BLF is applied to avoid the limits violation and keep all the states within the predefined bounds.

https://doi.org/10.1017/S0263574722001266 Published online by Cambridge University Press

3. BLFs

A specific property of the BLFs is high growth of such functions with approaching to the constrained bounds in the neighborhoods. This issue enables us to get the solution process at any inner point of the feasible set and to remain in the interior without taking particular care of the constraints [16]. Therefore, the following definition is of concern.

According to ref. [41], a BLF $\Upsilon(x)$ is a scalar function, defined in accordance with the system $\dot{x} = f(x)$ on an open region D containing the origin. This scalar function $\Upsilon(x)$ is continuous and positive-definite. It has continuous first-order partial derivatives at every point of D and with the property $\Upsilon(x) \to \infty$ as x approaches the boundary of D, meets $\Upsilon(x) \leq \beta, \forall t \geq 0$ as to the solution $\dot{x} = f(x)$ for $x(0) \in D$ and some positive constant β, which is related to the initial value of x. Parameter β is introduced to describe the upper bound of this function.

Remark 2. With respect to the Remark 1, the state space is split for each autonomous surface vessel into errors z_{1i} and z_{2i}, where z_{1i} is the state to be constrained and z_{2i} is the free state. The state z_{1i} requires the BLF Υ_i to prevent it from reaching the limits β_{1i}, while z_{2i} may involve a quadratic function. Here, based on Lemma 1, $\eta_i, \upsilon_i \in R^3$ are the states variables where η_i is required to meet $|\eta_i(t)| < \beta_{1i}, \forall t \geq 0$ with β_{1i} being a constrained bound. The following Lemma formalizes the result for general forms of BLFs to assure that the outputs or state constraints are not violated.

Lemma 3.1. (ref. [41]) *For any positive constants β_{1i} and β_{2i}, let $z_{1i} := \{z_{1i} \in : \beta_{1i} < z_{1i} < \beta_{2i}\} \subset R^3$. Consider the system*

$$\dot{\eta}_i = h(t, \eta), \tag{9}$$

where $\eta_i := [\omega_i, z_{1i}]^T$ and h is the piecewise continuous in t, locally Lipchitz in z and uniformly in t. Assume that there exists function $U_i : \Upsilon_i(z_{1i} \to R^+)$ continuously differentiable and positive-definite in their respective domains in a sense that

$$\Upsilon_i(z_{1i}) \to \infty \text{ as } z_{1i} \to -\beta_{1i} \text{ or } z_{1i} \to \beta_{1i}, \tag{10}$$

$$\gamma_{1i}(\|\omega_i\|) \leq U_i(\omega_i) \leq \gamma_{2i}(\|\omega_i\|), \tag{11}$$

where γ_{1i} and γ_{2i} are the class k_∞ functions. Let $\Upsilon_i(\eta) = \Upsilon_i(z_{1i}) + U_i(\omega_i)$ and the initial error $z_{1i}(0)$ belongs to the set $z_{1i} \in (-\beta_{1i}, \beta_{2i})$. If the following inequality holds true:

$$\dot{\Upsilon}_i = \frac{\partial \Upsilon}{\partial \eta} h \leq 0, \tag{12}$$

then the error $z_{1i}(t)$ remains in the open set $z_{1i} \in (-\beta_{1i}, \beta_{1i})\ \forall t \in [0, \infty)$.

Lemma 3.2. (ref. [42]) *For any positive constant β_{1i}, the following inequality holds for all errors z_{1i} in the interval $\|z_{1i}\| < \beta_{1i}$:*

$$\log \frac{\beta_{1i}^2}{\beta_{1i}^2 - z_{1i}^2} < \frac{z_{1i}^2}{\beta_{1i}^2 - z_{1i}^2}. \tag{13}$$

Assumptions: The following assumptions are essential to meet the mentioned control objectives:

1. Over the compact set $\upsilon_i \in \Omega_\upsilon$, the NN ideal weight vector θ_i^*, and the minimum approximation error $\delta_i^*(\upsilon_i)$ of NN are bounded through

$$\|\theta_i^*\| \leq \theta_{mi}, \quad \|\delta_i^*(\upsilon_i)\| \leq \varepsilon_i, \quad \forall \upsilon_i \in \Omega_{\upsilon i}, \tag{14}$$

   where θ_{mi} and ε_i are the positive constants.

2. The sway velocity ν_i is passive bound. This feature is systematically analyzed with respect to different cases in ref. [10]. This assumption is highly actual in practice because the hydrodynamic damping force is dominant in the sway direction which damps out the sway speed.

https://doi.org/10.1017/S0263574722001266 Published online by Cambridge University Press

3. The external disturbance τ_{di} acting on each surface vessel which is subjected to wind, wave and sea currents is bounded in practical engineering. Consequently, there exist a scalar $\Sigma_i \in R^+$ such that $\|\tau_{di}\| \leq \Sigma_i$.

Lemma 3.3. Finite-time theory (ref. [21]) *Consider the nonlinear system* $\dot{x}_i = f_i(x_i)$ *with both* $f_i(0) = 0$ *and* $x_i(0) = x_0$. *Provided that the function* $\Upsilon_i(x) : U_i \to R$ *is defined as continuously differentiable, positive-definite on a neighborhood and the time derivative of this function is obtained as:*

$$\dot{\Upsilon}_i(x) \leq -C_{1i}\Upsilon_i(x) - C_{2i}\Upsilon_i^{\mu_i}(x), \tag{15}$$

where $C_{1i}, C_{2i} > 0$ *and* $0 < \mu_i < 1$, *then the origin is locally finite-time stable. Provided that* $U_i = R^N$ *and* $\Upsilon_i(x)$ *are bounded in their radial sense, then the origin is globally finite-time stable. In this context, the finite-time* $T_i \in [0, \infty)$ *meets the following requirements based on the initial states:*

$$T_i \leq \frac{1}{C_{1i}(1-\mu_i)} Ln \frac{C_{1i}\Upsilon_i^{1-\mu_i}(x_0) + C_{2i}}{C_{2i}}. \tag{16}$$

Remark 3. In practice, unlike the original control systems, it is necessary for the closed-loop system to achieve finite-time stability. A slow convergence speed may require longer time for the autonomous surface vessels to reach the desired position, and high overshoot might result in a collision between the follower and its predecessor. Both the finite-time convergence and stabilization not only assure higher convergence rate but also guarantee a better disturbance rejection, higher accuracy and greater robustness against uncertainties.

4. Formation control design for autonomous surface vessels

4.1. Neural network approximator

According to the universal approximation property, radial basis function neural networks (RBFNNs) are widely applied to compensate structured uncertainties due to the fact that RBFNNs are capable to approximate smooth uncertain functions in many nonlinear systems such as autonomous surface vessels. To this end, a nonlinear function is approximated as follows:

$$\hat{f}_i(\upsilon_i) := \hat{\theta}_i^T \Phi_i(\upsilon_i), \tag{17}$$

where $\upsilon_i \in \Omega_{\upsilon i} \subset R^q$ is the input vector and q is the NN input dimension, $\hat{\theta}_i = [\hat{\theta}_{1i}, \hat{\theta}_{2i}, \ldots, \hat{\theta}_{li}]^T \in R^l$ is the NN weights vector and $l > 1$ is the NN number. The regression vector $\Phi_i(\upsilon_i) = [\varphi_{1i}(\upsilon_i), \ldots, \varphi_{li}(\upsilon_{li})]^T$ is the basis function vector where $\varphi_i(\upsilon_i)$ is defined as $\varphi_i(\upsilon_i) = \exp[\|\upsilon_i - \mu_i\|^2/c_i]$, $i = 1, \ldots, l$; where, $\mu_i = [\mu_{i1}, \ldots, \mu_{iq}]^T$ is the center of Gaussian functions and $c_i > 0$ is the width of them. For any unknown nonlinear function $f_i(\upsilon_i)$ that contains $C_i(\upsilon_i)$ and $D_i(\upsilon_i)$, there exists the NN function $\theta_i^{*T}\Phi_i(\upsilon_i)$ in a sense that

$$f_i(\upsilon_i) := \theta_i^{*^T}\Phi_i(\upsilon_i) + \delta_i^*(\upsilon_i), \quad \forall \upsilon_i \in \Omega_{\upsilon i} \in R^q, \tag{18}$$

where $\delta_i^*(\upsilon_i)$ is the minimum approximation error and θ_i^* is the ideal constant vector defined as:

$$\theta_i^* := \arg \min_{\hat{\theta}_i \in R^l} \sup\nolimits_{\upsilon_i \in \Omega_{\upsilon i}} f(\upsilon_i) - \hat{\theta}_i^T \Phi_i(\upsilon_i). \tag{19}$$

4.2. HGO

In some practical systems, the limitations and environmental disturbances together with technological limitations make accurate velocity measurements of surface vessels difficult [44]. A HGO is applied to estimate these unmeasurable states, referred to as υ_i for $i = 1, \ldots, N$. The dynamics of HGO are

https://doi.org/10.1017/S0263574722001266 Published online by Cambridge University Press

expressed as follows:

$$\begin{cases} m_i\dot{\lambda}_{i1} = \lambda_{i2} \\ m_i\dot{\lambda}_{i2} = -m_{1i}\lambda_{i2} - \lambda_{i1} + \eta_i \end{cases}, \tag{20}$$

where $\lambda_{i1}, \lambda_{i2} \in R^n$ are the state vectors of HGO, m_{1i} and m_i are the small positive constants. To prevent peaking, the saturation functions are applied to a given observer signal when it is outside the preferable range Ω as [46]:

$$\lambda_{ij} = \mathrm{B}_{ij}\Delta\left(\frac{\lambda_{ij}}{\mathrm{B}_{ij}}\right), \quad \mathrm{B}_{ij} \geq \max_{\upsilon\in\Omega_{\upsilon i}}(\lambda_{ij}), \tag{21}$$

where

$$\Delta(a) = \begin{cases} -1 & for\ a < -1 \\ a & for\ |a| \leq +1 \\ +1 & for\ a > +1 \end{cases}$$

Consequently, the following equation can be proved [45]:

$$\Lambda_{i2} = \frac{\lambda_{2i}}{m_i} - \upsilon_i = m_i\mathrm{X}_i^{(2)} \tag{22}$$

where $\mathrm{X}_i = \lambda_{i2} + m_i\lambda_{i1}$ and there exist positive constants t^* and g_{i2} in a sense that $\forall\, t > t^*$, $\|\Lambda_{i2}\| \leq \kappa_i g_{i2}$ holds true.

4.3. Output feedback adaptive-neural formation controller design

To design DSC for the formation control of surface vessels, the formation tracking errors are defined for the first and second steps through the state variables η_i and υ_i as:

$$\begin{cases} z_{1i} = \eta_i - \eta_0 \\ z_{2i} = \upsilon_i - \mathrm{P}_{iF} \end{cases} \quad i = 1, \ldots, N. \tag{23}$$

Let $z_{1i} = [z_{11i}, z_{12i}, z_{13i}]^T$ and $z_{2i} = [z_{21i}, z_{22i}, z_{23i}]^T$. With respect to the suggested HGO, the estimation of second surface errors in (23) is rewritten as:

$$\hat{z}_{2i} = \hat{\upsilon}_i - \mathrm{P}_{iF} = J^{-1}(\psi_i)\frac{\lambda_{2i}}{m_i} - \mathrm{P}_{iF}, \tag{24}$$

where P_{iF} is the virtual control signal that is passed through the following first-order filter:

$$\alpha_i\dot{\mathrm{P}}_{iF} + \mathrm{P}_{iF} = \mathrm{P}_i \qquad \mathrm{P}_{iF}(0) = \mathrm{P}_i(0), \tag{25}$$

where P_i is the virtual controller and α_i is a design parameter. Consequently, the following error is defined for each surface vessel in the formation control:

$$\mathrm{P}_{ie} = \mathrm{P}_{iF} - \mathrm{P}_i. \tag{26}$$

Next, one has the following equation through (25) and (26):

$$\dot{\mathrm{P}}_{ie} = \dot{\mathrm{P}}_{iF} - \dot{\mathrm{P}}_i = \frac{1}{\alpha_i}\mathrm{P}_{ie} - \dot{\mathrm{P}}_i. \tag{27}$$

Consequently, one may find that

$$\left\|\dot{\mathrm{P}}_{ie} + \frac{\mathrm{P}_{ie}}{\alpha_i}\right\| \leq \varpi, \tag{28}$$

https://doi.org/10.1017/S0263574722001266 Published online by Cambridge University Press

where ϖ is the continuous function of closed-loop variables and their derivatives that is used to derive the following inequality, where will be used in the stability analysis in the sequel:

$$\mathrm{P}_{ie}^{T}\dot{\mathrm{P}}_{ie} \leq -\frac{1}{\alpha_i}\|\mathrm{P}_{ie}\|^2 + \|\mathrm{P}_{ie}\|^2 + \frac{1}{4}\varpi^2. \tag{29}$$

In the second step, the virtual surface error of each surface vessel is obtained by

$$\tilde{z}_{2i} = \hat{z}_{2i} - z_{2i} = J^{-1}(\psi_i)\frac{\lambda_{2i}}{m_i} - \mathrm{P}_{iF} - \upsilon_i + \mathrm{P}_{iF} = \Lambda_{i2}. \tag{30}$$

With respect to the conditions of HGO and $\left\|J^{-1}\right\| \leq S_i$ where $S_i \in \Re^+$ is an unknown constant, the following inequalities are of concern:

$$\|\tilde{z}_2\| = \left\|J^{-1}(\eta)\left(\frac{\lambda_{i2}}{m_i} - \dot{\eta}\right)\right\| = \left\|J^{-1}(\eta)m_i\ddot{\chi}\right\| \leq m_i P_2\left\|J^{-1}(\eta)\right\| \leq m_i P_2 S_i := S_2, \tag{31}$$

$$\|\tilde{z}_2\|^2 = \left\|J^{-1}(\eta)\left(\frac{\lambda_{i2}}{m_i} - \dot{\eta}\right)\right\|^2 = \left\|J^{-1}(\eta)m_i\ddot{\chi}\right\|^2 \leq m_i^2 P_2^2\left\|J^{-1}(\eta)\right\|^2 \leq m_i^2 P_2^2 S_i^2 := S_2^2. \tag{32}$$

By replacing $\hat{\upsilon}_i = \hat{z}_{2i} + \mathrm{P}_{iF}$ and derivation from the calculated tracking errors, the following equations are obtained:

$$\begin{aligned} \dot{z}_{1i} &= J_i(\hat{z}_{2i} + \mathrm{P}_{iF}) - \dot{\eta}_0, \\ \dot{z}_{2i} &= \dot{\hat{\upsilon}}_i - \dot{\mathrm{P}}_{iF}. \end{aligned} \tag{33}$$

At this step, to facilitate discussion on the limited FOV constraint requirements of the formation tracking errors, the symmetric BLF is introduced for each surface vessel [22] as follows:

$$\Upsilon_{1i} = \frac{1}{2}\log\frac{\beta_{1i}^2}{\beta_{1i}^2 - z_{1i}^T z_{1i}}, \quad \|z_{1i}(0)\| < \beta_{1i}. \tag{34}$$

The derivative of the BLF is calculated based on the formation tracking errors of each surface vessel. By inserting the calculated dynamic error in the derivative of the BLF, the following equation is obtained:

$$\dot{\Upsilon}_{1i} = \frac{z_{1i}^T\dot{z}_{1i}}{\beta_{1i}^2 - z_{1i}^T z_{1i}} = \frac{z_{1i}^T(J_i(\psi_i)(\hat{z}_{2i} + \mathrm{P}_i) - \dot{\eta}_0)}{\beta_{1i}^2 - z_{1i}^T z_{1i}}. \tag{35}$$

Consequently, the virtual control signals are designed according to the BLF derivative and finite-time approach on the formation control of autonomous surface vessels as

$$\mathrm{P}_i = J_i^{-1}(\psi_i)(\dot{\eta}_0 - c_{1i}z_{1i}(\beta_{1i}^2 - z_{1i}^T z_{1i}) - c_{2i}\mathrm{sgn}^{\alpha}(z_{1i})), \tag{36}$$

where c_{1i} and c_{2i} are the designed positive parameters, $\mathrm{sgn}^{\alpha}(z_{1i}) = |z_{1i}|^{\alpha} sign(z_{1i})$ which $0.5 < \alpha < 1$. With substituting the virtual control (36) into (35), the following equation is obtained:

$$\dot{\Upsilon}_{1i} = \frac{J_i z_{1i}\hat{z}_{2i} - c_{1i}z_{1i}^2(\beta_{1i}^2 - z_{1i}^T z_{1i}) - c_{2i}z_{1i}\mathrm{sgn}^{\alpha}(z_{1i})}{\beta_{1i}^2 - z_{1i}^T z_{1i}}. \tag{37}$$

With respect to equation $z_{1i}sign(z_{1i}) = |z_{1i}|$, term $c_{2i}|z_{1i}|^{\alpha+1}$ is replaced into $c_{2i}z_{1i}\mathrm{sgn}^{\alpha}(z_{1i})$; thus, the following equation is achieved:

$$\dot{\Upsilon}_{1i} = -c_{1i}z_{1i}^2 + \frac{J_i z_{1i}\hat{z}_{2i}}{\beta_{1i}^2 - z_{1i}^T z_{1i}} - \frac{c_{2i}|z_{1i}|^{\alpha+1}}{\beta_{1i}^2 - z_{1i}^T z_{1i}}. \tag{38}$$

By applying a simple math calculations, the following equation is obtained:

$$\dot{\Upsilon}_{1i} = -c_{1i}z_{1i}^2 + \frac{J_i z_{1i}\hat{z}_{2i}}{\beta_{1i}^2 - z_{1i}^T z_{1i}} - c_{2i}(\beta_{1i}^2 - z_{1i}^T z_{1i})^{\frac{\alpha-1}{2}}\left(\frac{z_{1i}^2}{\beta_{1i}^2 - z_{1i}^T z_{1i}}\right)^{\frac{\alpha+1}{2}}. \tag{39}$$

https://doi.org/10.1017/S0263574722001266 Published online by Cambridge University Press

According to Lemma 1, we have $\frac{1}{2}\log\frac{\beta_{1i}^2}{\beta_{1i}^2 - z_{1i}^T z_{1i}} < \frac{z_{1i}^2}{2(\beta_{1i}^2 - z_{1i}^T z_{1i})}$. Let $\rho_{1i} = \beta_{1i}^2 - z_{1i}^T z_{1i}$ which is positive, then, the following equation is obtained:

$$\dot{\Upsilon}_{1i} = -2c_{1i}\rho_{1i}\Upsilon_{1i} - c_{2i}\rho_{1i}^{\frac{\alpha-1}{2}}(2\Upsilon_{1i})^{\frac{\alpha+1}{2}} + \frac{J_i z_{1i}\hat{z}_{2i}}{\beta_{1i}^2 - z_{1i}^T z_{1i}}. \tag{40}$$

Remark 4. An extra term $-c_{2i}\mathrm{sgn}^{\alpha}(z_{1i})$ in the virtual control (36) is proposed for the finite-time stability which would increase the convergence rate and accuracy. Because of to $0.5 < \alpha < 1$, the derivatives of this term may lead to singularity problem on the error surface. Consequently, to overcome this drawback, the first-order SMD which can engulf the derivatives of the virtual control laws which are applied to the DSC approach.

After designing the virtual control singals for each surface vessel in step 1, the quadratic Lyapunov function is proposed in step 2 as follows:

$$\Upsilon_{2i} = \Upsilon_{1i} + \frac{1}{2}z_{2i}^T M_i z_{2i} + \frac{1}{2\gamma_i}\tilde{\theta}_i^T\tilde{\theta}_i + \frac{1}{2}\mathrm{P}_{ie}^T\mathrm{P}_{ie}, \tag{41}$$

where $\gamma_i > 0$ is a design parameter and $\tilde{\theta}_i = \theta_i^* - \hat{\theta}_i$. By calculating the derivative of Lyapunov function in step 2, the following equation is obtained:

$$\dot{\Upsilon}_{2i} = \dot{\Upsilon}_{1i} + z_{2i}^T M_i \dot{z}_{2i} - \frac{1}{\gamma_i}\tilde{\theta}_i^T\dot{\hat{\theta}}_i + \mathrm{P}_{ie}^T\dot{\mathrm{P}}_{ie}. \tag{42}$$

By inserting the error dynamic into this derivative, the following result is achieved:

$$\begin{aligned}\dot{\Upsilon}_{2i} = {} & -2c_{1i}\rho_{1i}\Upsilon_{1i} - c_{2i}\rho_{1i}^{\frac{\alpha-1}{2}}(2\Upsilon_{1i})^{\frac{\alpha+1}{2}} + \frac{J_i z_{1i}^T\hat{z}_{2i}}{\beta_{1i}^2 - z_{1i}^T z_{1i}} \\ & + z_{2i}^T(-C_i(\upsilon_i)z_{2i} - D_i(\upsilon_i)z_{2i} + \tau_i + f_i^*(\upsilon_i)) - \frac{1}{\gamma_i}\tilde{\theta}_i^T\dot{\hat{\theta}}_i + \mathrm{P}_{ie}^T\dot{\mathrm{P}}_{ie},\end{aligned} \tag{43}$$

where $f_i^*(\upsilon_i) = -C_i(\upsilon_i)\mathrm{P}_{iF} - D_i(\upsilon_i)\mathrm{P}_{iF} - G_i(\eta_i) - M_i\dot{\mathrm{P}}_{iF}$. By inserting $f_i^*(\upsilon_i) = \theta_i^{*T}\varphi_i + \varepsilon_i$ into Eq. (43), where ε_i is the approximator error in the derivative of Lyapunov function in step 2, the following is yield:

$$\begin{aligned}\dot{\Upsilon}_{2i} = {} & -2c_{1i}\rho_{1i}\Upsilon_{1i} - c_{2i}\rho_{1i}^{\frac{\alpha-1}{2}}(2\Upsilon_{1i})^{\frac{\alpha+1}{2}} + \frac{J_i z_{1i}^T\hat{z}_{2i}}{\beta_{1i}^2 - z_{1i}^T z_{1i}} \\ & + z_{2i}^T\Big(-C_i(\upsilon_i)\,z_{2i} - D_i(\upsilon_i)z_{2i} + \tau_i + \tilde{\theta}_i^T\varphi_i + \hat{\theta}_i^T\varphi_i + \varepsilon_i\Big) - \frac{1}{\gamma_i}\tilde{\theta}_i^T\dot{\hat{\theta}}_i \\ & - \left(\frac{1}{\alpha_i} - 1 - 0.5\lambda_{\max}\{J_i(\psi_i)\}\right)\|\mathrm{P}_{ie}\|^2 + \frac{1}{4}\varpi^2.\end{aligned} \tag{44}$$

The sigma-modification structure is utilized as a robust adaptive law until it makes the estimated parameters to become fixed at specific points. The adaptive laws are chosen for each surface vessel as follows:

$$\dot{\hat{\theta}}_i = \gamma_i z_{2i}^T\varphi_i - \gamma_i\delta_i(\hat{\theta}_i - \theta_{i0}), \tag{45}$$

where $\gamma_i > 0$ and $\delta_i > 0$ are the design parameters. The parameters $\theta_{i0} \in R^3$ are priori estimates of the parameters θ_i. Consequently, the formation control signal for each surface vessel is designed as:

$$\tau_i = -c_{3i}\hat{z}_{2i} - c_{4i}sig^{\alpha}(\hat{z}_{2i}) - \hat{\theta}_i^T\varphi_i - \frac{J_i z_{1i}}{\beta_{1i}^2 - z_{1i}^T z_{1i}} - \hat{\tau}_{di}, \tag{46}$$

where parameters c_{3i} and c_{4i} are the designed positive constants and $\hat{\tau}_{di}$ will be designed as the finite-time disturbance observer in the next step. With respect to $z_{2i}^T\big(\dot{M}_i - 2C_i(\upsilon_i)\big)\,z_{2i} = 0$ and by substituting the

https://doi.org/10.1017/S0263574722001266 Published online by Cambridge University Press

control signals into the derivative of Lyapunov function, the following equation is obtained:

$$\begin{aligned}\dot{\Upsilon}_{2i} = &-2c_{1i}\rho_{1i}\Upsilon_{1i} - c_{2i}\rho_{1i}^{\frac{\alpha-1}{2}}(2\Upsilon_{1i})^{\frac{\alpha+1}{2}} - z_{2i}^T c_{3i} z_{2i} - z_{2i}^T c_{3i}\tilde{z}_{2i} \\ &-c_{4i}\left(\|z_{2i}\|^2\right)^{\frac{\alpha+1}{2}} - c_{4i}\left(\|\tilde{z}_{2i}\|^2\right)^{\frac{\alpha+1}{2}} - z_{2i}^T D_i z_{2i} + z_{2i}^T \varepsilon_i + \tilde{\theta}_i^T \delta_i(\hat{\theta}_i - \theta_{i0}) \\ &-\left(\tfrac{1}{\alpha_i} - 1 - 0.5\lambda_{\max}\{J_i(\psi_i)\}\right)\mathrm{P}_{ie}{}^2 + \tfrac{1}{4}\varpi^2.\end{aligned} \tag{47}$$

With respect to inequalities (29) and (32) and through assumption $\varepsilon_i{}^2 < \varepsilon_i^{*2}$ and Lemma 2, the following inequalities can be obtained by applying the Young's inequality as follows:

$$z_{2i}^T \varepsilon_i \le \frac{1}{2} z_{2i}^T z_{2i} + \frac{1}{2}\varepsilon_i^{*2}, \tag{48}$$

$$\tilde{\theta}_i^T \delta_i(\hat{\theta}_i - \theta_{i0}) \le -(1 - 0.5/k^2)\delta_i \left\|\tilde{\theta}_i\right\|^2 + 0.5\delta_i\|\theta_i - \theta_{i0}\|^2, \tag{49}$$

$$-z_{2i}^T c_{3i}\tilde{z}_{2i} \le 0.5\lambda_{\max}\{c_{3i}\}\,\|z_{2i}\|^2 + 0.5\lambda_{\max}\{c_{3i}\}\,\|\tilde{z}_{2i}\|^2. \tag{50}$$

Consequently, with replacing the inequalities (48)–(50) into Eq. (47), the following inequality is achieved:

$$\begin{aligned}\dot{\Upsilon}_{2i} \le &-2c_{1i}\rho_{1i}\Upsilon_{1i} - c_{2i}\rho_{1i}^{\frac{\alpha-1}{2}}(2\Upsilon_{1i})^{\frac{\alpha+1}{2}} - \rho_{2i}\|\mathrm{P}_{ie}\|^2 - \rho_{5i}\|z_{2i}\|^2 \\ &-c_{4i}\left(\|z_{2i}\|^2\right)^{\frac{\alpha+1}{2}} - \rho_{3i}\left\|\tilde{\theta}_i\right\|^2 + \tfrac{1}{2}\varepsilon_i^{*2} + \rho_{4i} + \rho_{6i},\end{aligned} \tag{51}$$

where parameters $\rho_{2i} = \left(\frac{1}{\alpha_i} - 1 - \lambda_{\max}(J_i(\psi_i))\right)$, $\rho_{3i} = (1 - 0.5/k^2)\delta_i$, $\rho_{4i} = 0.5\delta_i\|\theta_i - \theta_{i0}\|^2$, $\rho_{5i} = \lambda_{\min}\{D_i + c_{3i} + c_{4i}\} - 0.5\lambda_{\max}\{c_{3i}\}$ and $\rho_{6i} = \frac{S_2^2}{2} + \frac{1}{4}\varpi^2$ are positive constants with conditions $\lambda_{\min}\{D_i + c_{3i} + c_{4i}\} > 0.5\lambda_{\max}\{c_{3i}\}$ and $\frac{1}{\alpha_i} > 1 + \lambda_{\max}(J_i(\psi_i))$.

Remark 5. Since in the constrained formation control problem, each ASV can only acquire the position information from its immediate predecessor, such position states of ASVs are unmeasurable and the tracking errors can be considered in the predefined and constrained bounds which are time-varying by recalling the limited FOV. To satisfy these constraints on the formation tracking errors, the following constraints are considered:

$$\underline{\beta}_i(t) \le z_i(t) \le \bar{\beta}_i(t) \tag{52}$$

with

$$\begin{aligned}\bar{\beta}_i(t) &= \bar{\beta}_{i,\infty} + (\bar{\beta}_{i,0} - \bar{\beta}_{i,\infty})e^{-k_i t}, \\ \underline{\beta}_i(t) &= \underline{\beta}_{i,\infty} + (\underline{\beta}_{i,0} - \underline{\beta}_{i,\infty})e^{-k_i t},\end{aligned} \tag{53}$$

where $\bar{\beta}_{i,0}$, $\bar{\beta}_{i,\infty}$, $\underline{\beta}_{i,0}$, $\underline{\beta}_{i,\infty}$ and k_i are the positive design parameters, $\bar{\beta}_i(t)$ and $\underline{\beta}_i(t)$ are the maximum and minimum allowable tracking errors with $\bar{\beta}_{i,\infty} \le \bar{\beta}_{i,0}$ and $\underline{\beta}_{i,\infty} \le \underline{\beta}_{i,0}$, respectively. These time-varying boundaries of the tracking errors are utilized in the conversion of the error transformation.

The asymmetric BLFs are proposed to assure the time-varying limited FOV errors constrained within certain bounds such that leaders and followers can preserve the predefined structure and ensure the desired steady-state bounds as follow:

$$\Upsilon_i = \frac{q_z(z_i)}{2}\log\frac{\overline{\beta}_i^2}{\overline{\beta}_i^2 - z_i^2} + \frac{1 - q_z(z_i)}{2}\log\frac{\underline{\beta}_i^2}{\underline{\beta}_i^2 - z_i^2}, \tag{54}$$

where q_z is the logic variable which is equal to one if the kinematic error z_i is positive and the otherwise is equal to zero; $\underline{\beta}_i$ and $\overline{\beta}_i$ are the minimum and maximum constraints on the time-varying error z_i,

https://doi.org/10.1017/S0263574722001266 Published online by Cambridge University Press

respectively. To dominate the time dependency, the following conversion of variables is proposed:

$$\Omega_{z1} = \frac{z_i}{\beta_i}, \quad \Omega_{z2} = \frac{z_i}{\beta_i}, \quad \Omega_z = q_z\Omega_{z2} + (1 - q_z)\Omega_{z1}. \tag{55}$$

With the above conversion of coordinates, the BLF Υ_i is rewritten without the time dependency as follows:

$$\Upsilon_i = \frac{1}{2}\log\frac{1}{1 - \Omega_z^2}. \tag{56}$$

It is obvious that the BLF Υ_i is positive-definite and continuously differentiable in the set $|\Omega_z| < 1$. This suggested BLF based on the error transformation can be substituted into the proposed BLF in Eq. (34) with respect to the time-varying predefined and limited FOV constraints.

4.4. Terminal sliding-mode disturbance observer design

The environmental disturbances vector τ_{di} is bounded and not measurable precisely in practice, indicating that the designed terminal sliding-mode disturbance observer has more practical value. The physical meanings of these imposed environmental disturbances are mostly due to the sea and ocean currents, storms, waves and winds. However, its interpretation may generally cover strong couplings, uncertain nonlinearities, modeling errors and unmodeled dynamics of the system. In this step, a terminal sliding-mode observer-based estimation scheme will be developed more to assure the actual external disturbance for each surface vessel to allow high-accuracy estimation after finite-time. To design an estimation law for disturbance τ_{di}, the new error variable $\Xi_i = \upsilon_i - \Phi_i$ is introduced firstly for each surface vessel where $\Phi_i \in R^3$ is updated through the following equation:

$$\Phi_i = M_i^{-1}(K_{i1}\Xi_i + K_{i2}\mathrm{sgn}(\Xi_i) + \tau_i - C_i(\upsilon_i)\upsilon_i - D_i(\upsilon_i)\upsilon_i - g_i(\eta_i)). \tag{57}$$

This nonlinear terminal sliding-mode disturbance observer estimation law is implemented in the control design to obtain in a high performance control against external disturbances through finite-time convergence of tracking errors vector for each surface vessel into a compact set as:

$$\hat{\tau}_{di} = K_{1i}\Xi_i + K_{2i}\mathrm{sgn}(\Xi_i) \tag{58}$$

where K_{1i} and K_{2i} are positive constants. The actual τ_{di} can be estimated precisely through $\hat{\tau}_{di}$. Moreover, the estimated disturbance error $e_{di} = \hat{\tau}_{di} - \tau_{di}$ for each surface vessel is assured to converge to zero in an asymptotic manner. In practice, to reduce the chattering in the finite-time convergence, a continuous function $\Xi_i/(\|\Xi_i\| + \varepsilon_i)$ must be adopted to approximate the $\mathrm{sgn}(\Xi_i)$ function. This designed terminal sliding-mode disturbance observer is implemented without any assumption on the upper bound of disturbances in the control design to increase the control system performance.

To prove the convergence of this terminal sliding-mode disturbance observer law, the following Lyapunov function is proposed for each surface vessel:

$$\Upsilon_{3i} = 0.5\ \Xi_i^T M_i \Xi_i. \tag{59}$$

With respect to Eq. (4), control signal (46) and terminal sliding-mode law (53), the following equation is yielded:

$$\begin{aligned} M_i\dot{\Xi}_i &= M_i\dot{\upsilon}_i - M_i\dot{\Phi}_i \\ &= -K_{i1}\Xi_i - K_{i2}\mathrm{sgn}(\Xi_i) + \tau_{id}. \end{aligned} \tag{60}$$

The time derivative of Lyapunov function (59) is calculated along with disturbance observer error Ξ_i as:

$$\begin{aligned} \dot{\Upsilon}_{3i} &= \Xi_i^T(\tau_{di} - K_{i1}\Xi_i - K_{i2}\mathrm{sgn}(\Xi_i) - K_{i3}\lfloor\Xi_i\rfloor^{p_i/q_i}) \\ &\le -K_{i1}\|\Xi_i\|^2 - K_{i2}\|\Xi_i\| + \Sigma_i\|\Xi_i\| - K_{i3}\Xi_i^T\lfloor\Xi_i\rfloor^{p_i/q_i} \\ &\le -K_{i1}\|\Xi_i\|^2 - K_{i3}\Xi_i^T\lfloor\Xi_i\rfloor^{p_i/q_i} \end{aligned} \tag{61}$$

https://doi.org/10.1017/S0263574722001266 Published online by Cambridge University Press

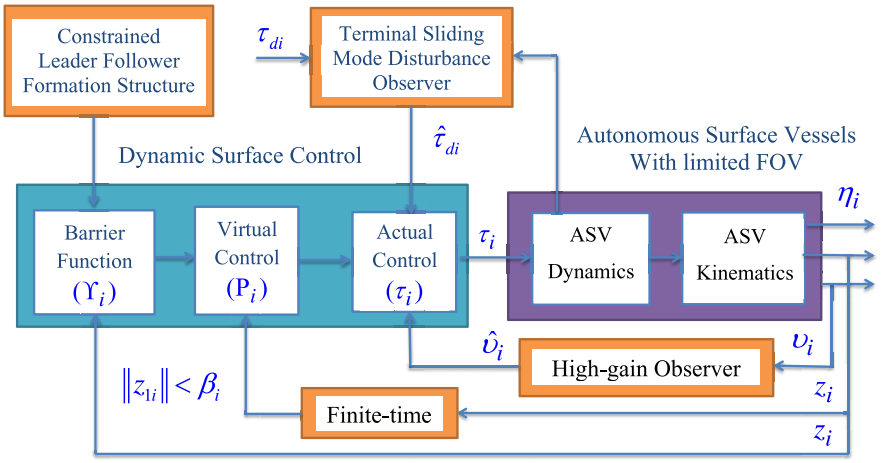

Figure 2. *Suggested block diagram for the leader-follower formation control of autonomous surface vessels.*

With applying Lemma 1, the inequality (61) will be bounded more through:

$$\dot{\Upsilon}_{3i} \leq -\frac{2K_{i1}}{\lambda_{\max}(M_i)}\Upsilon_{3i} - K_{3i}\left(\frac{2}{\lambda_{\max}(M_i)}\right)^{\sigma}(\Upsilon_{3i})^{\sigma} \tag{62}$$

where $\sigma = \dfrac{p_i + q_i}{2q_i}$. Consequently, $\dot{\Upsilon}_{3i}(t) \equiv 0$ for all convergence rate $t \geq t_{ix}$, which, t_{ix} is obtained through the following inequality at finite-time [43].

$$t_{ix} \leq \frac{1}{c(1+\alpha)} \ln \frac{c\Upsilon_{3i}^{1-\alpha}(0) + \iota_i}{\iota_i} \tag{63}$$

where $\iota_i = \dfrac{2K_{i1}}{\lambda_{\max(M_i)}}$ and $c_i = K_{i3}\left(\dfrac{2}{\lambda_{\max(M_i)}}\right)^{\sigma_i}$.

Consequently, it can be deduced that $\Upsilon_{3i} \equiv 0$, where $\dot{\Xi}_i = 0$, $t \geq t_{ix}$ and the disturbance estimation error e_{di} meets

$$\begin{aligned} e_{di} &= K_{i1}\Xi_i + K_{i2}\mathrm{sgn}(\Xi_i) + K_{i3}\lfloor \Xi_i \rceil^{p_i/q_i} - (M_i\upsilon_i + C_i(\upsilon_i)\upsilon_i - \tau_i + D_i(\upsilon_i)\upsilon_i + G(\eta_i)) \\ &= M_i(-\dot{\upsilon}_i + \dot{\Phi}_i). \end{aligned} \tag{64}$$

As a result, $e_{di} = -M_i\dot{\Xi}_i$, which is finite-time stable, $e_{di} \equiv 0$, $t \geq t_{ix}$. Thus, the states of the closed-loop control system converge to the origin in finite-time and the estimation parameters are bounded. This suggested control structure is illustrated for the leader-follower formation control of autonomous surface vessels in Fig. 2.

Remark 6. In comparison with ref. [32], where the leader-follower performed based on range and bearing constraints, in this article, the leader-follower formation control accomplished based on the tracking error constraints. Moreover, since the control approach is based on finite-time, the finite-time disturbance observer is applied in this article which increases the disturbance rejection powerfully and improves both the high tracking precision and fast convergence rate in the formation control problem.

Remark 7. The negligence of the effects of external ocean disturbances in the formation control problem may lead to the system instability and collision of ASVs. Therefore, the finite-time terminal sliding-mode disturbance observer is proposed in this article to compensate such disturbances in the dynamics of all ASVs. This suggested finite-time disturbance observer-based controller for ASVs picks up the previous restrictions on the number of ASVs and the formation arrangement.

https://doi.org/10.1017/S0263574722001266 Published online by Cambridge University Press

Theorem 4.1. *Consider a group of cooperative autonomous surface vessels with kinematic and dynamic equations which are given by (1) and (4). Subjected to Assumptions 1-3 and constraint (7), the proposed control law (46) with applying HGO (20)-(22), adaptive law (45) and nonlinear disturbance observer (53) ensure that all the signals in the closed-loop control system remain bounded as $t \to \infty$ and the tracking errors $z_{1i}(t)$ and $z_{2i}(t)$ are semi-globally uniformly ultimately bounded (SGUUB) and converge into a small ball including the zero.*

Proof. Consider the following Lyapunov function for the overall formation control system:

$$\Upsilon_T(t) = \sum_{i=1}^{N} \left(\frac{1}{2} \log \frac{\beta_{1i}^2}{\beta_{1i}^2 - z_{1i}^T z_{1i}} + \frac{1}{2} z_{2i}^T M_i \, z_{2i} + \frac{1}{2\gamma_i} \tilde{\theta}_i^T \tilde{\theta}_i + \frac{1}{2} \mathrm{P}_{ie}^T \mathrm{P}_{ie} + \frac{1}{2} \, \Xi_i^T M_i \, \Xi_i \right). \tag{65}$$

The following inequality is obtained for the entire formation control system:

$$\begin{aligned} \dot{\Upsilon}_T(t) \leq \sum_{i=1}^{N} \Bigg(& -2c_{1i}\rho_{1i}\Upsilon_{1i} - c_{2i}\rho_{1i}^{\frac{\alpha-1}{2}} (2\Upsilon_{1i})^{\frac{\alpha+1}{2}} - \rho_{2i} \|\mathrm{P}_{ie}\|^2 - \rho_{3i} \left\| \tilde{\theta}_i \right\|^2 - \rho_{5i} \|z_{2i}\|^2 \\ & - c_{4i} \left(\|z_{2i}\|^2 \right)^{\frac{\alpha+1}{2}} + \tfrac{1}{2} \varepsilon_i^{*2} + \rho_{4i} + \rho_{6i} - \frac{2K_{i1}}{\lambda_{\max}(M_i)} \Upsilon_{3i} - K_{3i} \left(\frac{2}{\lambda_{\max}(M_i)} \right)^{\sigma} (\Upsilon_{3i})^{\sigma} \Bigg). \end{aligned} \tag{66}$$

Consequently, inequality (66) can be represented for the overall formation control of autonomous surface vessels as follows:

$$\dot{\Upsilon}_T(t) = \sum_{i=1}^{N} \left(-s_i \|\chi_{ti}(t)\|^2 + \gamma_i(t) \right) \leq -s_{\min} \|\chi_t(t)\|^2 + \gamma(t), \tag{67}$$

where $\chi_{ti} = [z_{1i}^T, z_{2i}^T, \tilde{\theta}_i^T, \mathrm{P}_{ie}, \Xi_i^T]$, $\chi_t = [\chi_{t1}^T, \chi_{t2}^T, \ldots, \chi_{tN}^T]^T$, $s_{\min} = \min\{s_i\}_{i=1}^N$ and $\gamma(t) = \sum_{i=1}^{N} \gamma_i(t)$. In this context, ξ_i and γ_i are defined as follows:

$$\xi = \min \left\{ 2c_{1i}\rho_{1i}, c_{2i}\rho_{1i}^{\frac{\alpha-1}{2}}, \rho_{2i}, \rho_{5i}, \rho_{3i}, c_{4i}, \frac{2K_{i1}}{\lambda_{\max}(M_i)}, K_{3i} \left(\frac{2}{\lambda_{\max}(M_i)} \right)^{\sigma} \right\}. \tag{68}$$

$$\gamma = \rho_{4i} + \rho_{6i} + \frac{1}{2} \varepsilon_i^{*2}. \tag{69}$$

Consequently, with respect to definitions (68) and (69), the following inequality is obtained for the overall formation control of autonomous surface vessels:

$$\dot{\Upsilon}_T(t) \leq -\xi \, \Upsilon_T(t) + \gamma, \tag{70}$$

which assures that the closed-loop control system is SGUUB. According to Lemma 1, inequality $\|z_{1i}(t)\| < \beta_{1i} \; \forall t > 0$ yields that the initial conditions $\|z_{1i}(0)\| < \beta_{1i}$ are satisfied. Hence, it is known that $\eta_i(t) = z_{1i}(t) + \eta_0(t)$, $\|z_{1i}(t)\| < \beta_{1i}$ and $\|\eta_0(t)\| \leq A_0$, consequently, $\|\eta_i(t)\| < \beta_{1i} + A_0$ and the position output constraints will never be violated. The signals $z_i(t) = [z_{1i}(t), z_{2i}(t), z_{3i}(t)]^T$ remain in a defined bounded compact set through:

$$\Omega_z = \left\{ z_i \in R^n : |z_{1i}| \leq \beta_{1i}^2 \sqrt{1 - e^{-2\Upsilon_{1i}}}, \|z_{2i}\| \leq \sqrt{\frac{\max\left\{ \Upsilon(t_0), \frac{\gamma_i}{s_i} \right\}}{\lambda_{z_{\min}}}} \right\}. \tag{71}$$

This equation indicates that $\|z_i(t)\|$ decreases whenever $z_i(t)$ is outside the set Ω_z, revealing that $z_i(t)$ is SGUUB and converges exponentially to a neighborhood of the origin which assures that the leader-follower formation control system for the surface vessels under output constraints is SGUUB. By the function approximation capability of NNs, an adaptive-neural formation controller is designed for each surface vessel in a sense that all of them can synchronize the leader with tracking errors by being SGUUB in an asymptotic manner. Thus, all the signals in the closed-loop system are bounded and the tracking

https://doi.org/10.1017/S0263574722001266 Published online by Cambridge University Press

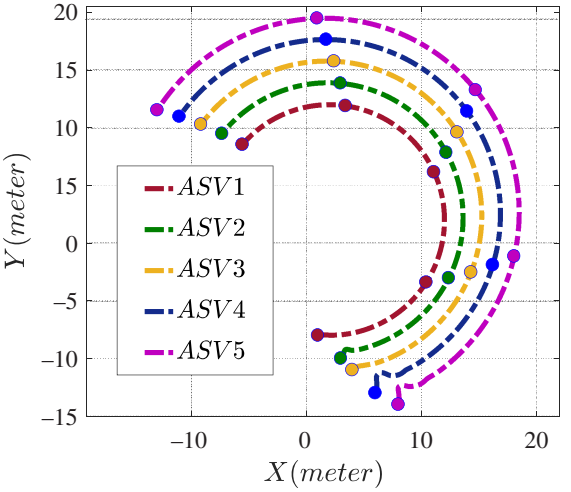

Figure 3. *Formation control of autonomous surface vessels with circle desired trajectory.*

errors converge to a small neighborhood of the origin by choosing the design parameters appropriately. Consequently, the obtained proof process is analogous to theorem. The proposed control method not only can guarantee the formation objective achieved within finite settling time but also can estimate the external disturbances in the finite-time. It is easy to draw the conclusion that the formation control problem of surface vessels can be solved with constrained states. □

5. Simulation results

To illustrate the performance of this newly proposed disturbance observer-based finite-time formation controller, a simulation of $N = 5$ identical models of the autonomous surface vessels is carried out where the system parameters are obtained from ref. [19]. Undoubtedly, there exist some model uncertainties and time-varying disturbances that are introduced in this model. The objective here is to make the formation control to achieve the desired trajectory to form the circle shapes with a radius of $12m$ with $\eta_0 = [2, -8, -1.5]^T$ for autonomous surface vessels, while avoiding from violation of constraints in the presence of uncertainties and disturbances. The initial positions and orientation of each surface vessel are represented by $\eta_1(0) = [1, -8, -1]^T$, $\eta_2(0) = [3, -10, -1.5]^T$, $\eta_3(0) = [4, -11, -1]^T$, $\eta_4(0) = [6, -13, -1]^T$, $\eta_5(0) = [8, -14, -1]^T$, which meet Lemma 1, and the initial velocities are $\upsilon_i(0) = [0, 0, 0]^T$. The formation trajectory of autonomous surface vessels in 2-D plane is illustrated in Fig. 3 where the followers have to follow the leaders at the finite-time in the presence of state constraints, external disturbances and uncertainties.

The constant coefficient of the first-order filter is considered as $\alpha_i = 0.005$; the virtual and actual controller coefficients $c_{1i} = 50$, $c_{2i} = 40$, $c_{3i} = 2$, $c_{4i} = 3$ are designed; the finite-time coefficient is considered as $\alpha = 0.85$; the high-gain velocity observer parameters are considered as $m_i = 0.2$, $m_{1i} = 5$; The designed disturbance observer parameters are selected as $K_{1i} = 60$, $K_{2i} = 20$, $\delta_i = 5$; the constraint bound for the formation tracking errors are selected as $\beta_{1i} = 0.05$. The initial estimated RBFNN parameters are selected as $\theta_{1i}(0) = 10$, $\theta_{2i}(0) = 2$ and $\theta_{3i}(0) = 1$ in the formation control of each autonomous surface vessel. Moreover, the time-varying reign of tracking errors regarding the limited FOV bound is suggested as $\bar{z}_{i,0} = +1$, $\bar{z}_{i,\infty} = +0.05$, $\underline{z}_{i,0} = -1$, $\underline{z}_{i,\infty} = -0.05$ and the exponential rate coefficient is selected as $k_i = 2$.

The designed actual control signals of autonomous surface vessels τ_{ui}, τ_{vi} and τ_{ri} are shown in Fig. 4. The high-gain velocity observer errors $\tilde{\upsilon}_{ui}$, $\tilde{\upsilon}_{vi}$ and $\tilde{\upsilon}_{ri}$ are illustrated in Fig. 5. It is clear that all signals are saturated due to the initial tracking error as well as the effects of HGO approximation. The distances and angles between autonomous surface vessels ρ_i, ψ_i are shown in Fig. 6. The disturbance observer

https://doi.org/10.1017/S0263574722001266 Published online by Cambridge University Press

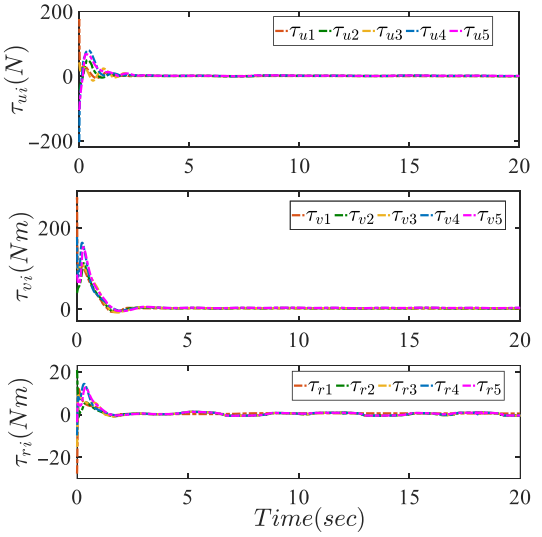

Figure 4. *Actual control signals of each autonomous surface vessels τ_{ui}, τ_{vi} and τ_{ri}.*

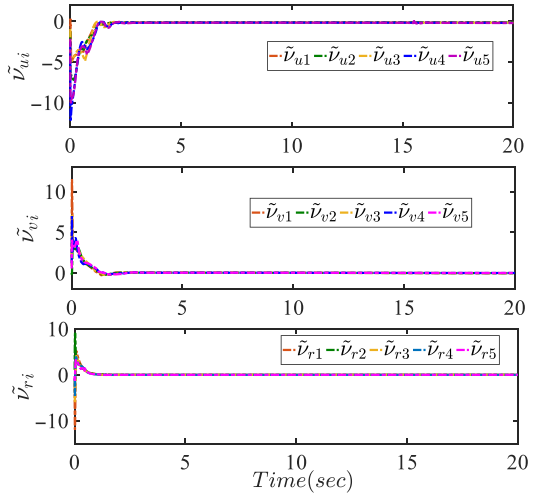

Figure 5. *High-gain velocity observer errors of the autonomous surface vessels $\tilde{\upsilon}_{ui}$, $\tilde{\upsilon}_{vi}$ and $\tilde{\upsilon}_{ri}$.*

output in the formation control is shown in Fig. 7. The disturbance observer errors of all ASVs Ξ_{d1i}, Ξ_{d2i}, Ξ_{di3} are shown in Fig. 8. The first surface errors of each ASV z_{xi}, z_{yi}, $z_{\psi i}$ and the second surface errors of each ASV z_{ui}, z_{vi} and z_{ri} are illustrated in Figs. 9 and 10, respectively.

The Frobenious norm of estimated NN parameters is illustrated in Fig. 11. An appropriate increasing of the NN nodes number will lead to a smaller approximation error, thus a decreasing in compact set Ω_i. This fact indicates that the formation is performed well despite the available time-varying disturbances and uncertainties. All surface vessels successfully track the leader to construct the desired formation without violating the constraints and the formation tracking performance of the cooperative autonomous surface vessels is met at finite-time.

As it can be seen in the Fig. 5, the HGO estimates the velocities of all ASVs in the finite settling time within about 2 s. It is clear that these estimates arrive at their respective saturation values and converge quickly to the actual output derivatives in a small neighborhood of their values.

https://doi.org/10.1017/S0263574722001266 Published online by Cambridge University Press

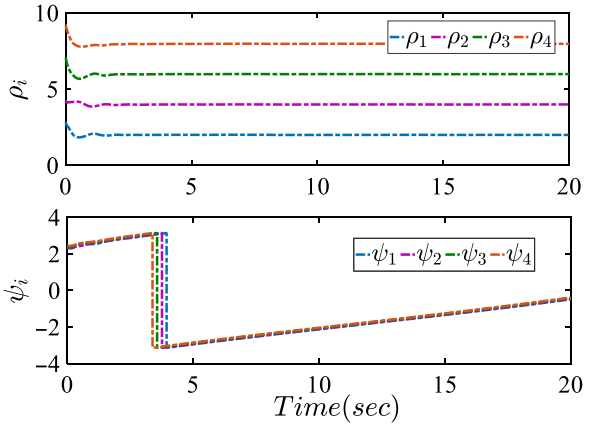

Figure 6. *Distances and orientation angles between the autonomous surface vessels ρ_i and ψ_i.*

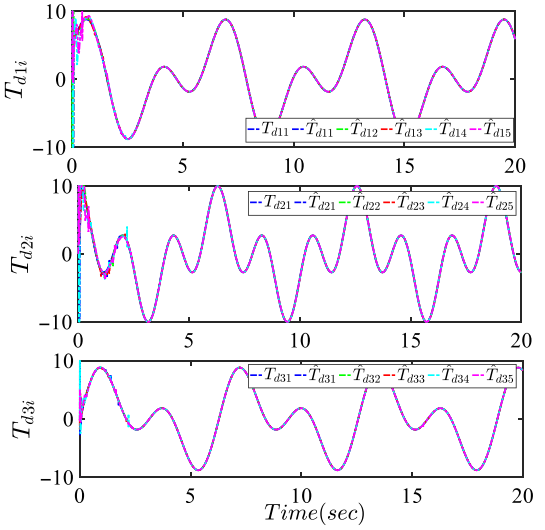

Figure 7. *Disturbance observer output of the autonomous surface vessels τ_{d1i}, τ_{d2i} and τ_{di3}.*

The external disturbance signals and the disturbance observer signals of all ASVs τ_{d1i}, τ_{d2i} and τ_{di3} are illustrated by Fig. 12. Also, the disturbance observer errors of all ASVs Ξ_{d1i}, Ξ_{d2i}, Ξ_{di3} are shown in Fig. 13. Moreover, the first error surface signals of all ASVs z_{xi}, z_{yi} and $z_{\psi i}$ in the presence of the external disturbances are illustrated by Fig. 14. It can be seen from Fig. 12 that the proposed disturbance observer (58) could process the disturbance estimations of all ASVs successfully in $t_{ix} = 2s$ according to (63).

5.1. A comparative experiment

To verify the performance of the suggested controller for the formation control of surface vessels, four scenarios are considered in this study. In the first scenario, the simulation is carried out for the DSC approach. In the second scenario, the BLF-based design is implemented in the suggested controller. In the third scenario, the finite-time technique is applied to the DSC approach, and in the fourth scenario, both BLF and finite-time strategies are utilized in the proposed control system. To compare between

https://doi.org/10.1017/S0263574722001266 Published online by Cambridge University Press

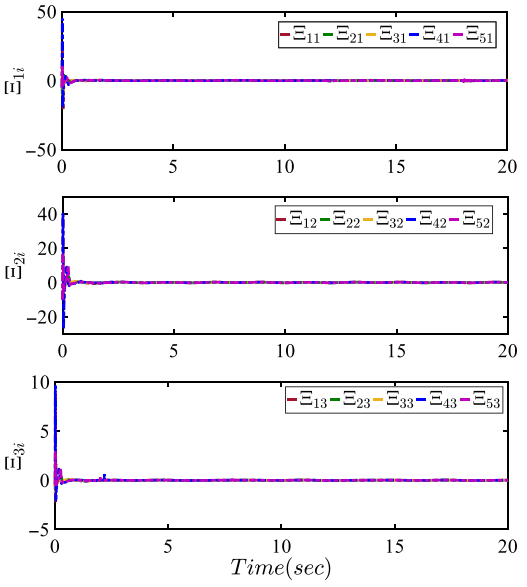

Figure 8. *Disturbance observer errors of the autonomous surface vessels* Ξ_{d1i}, Ξ_{d2i} *and* Ξ_{di3}.

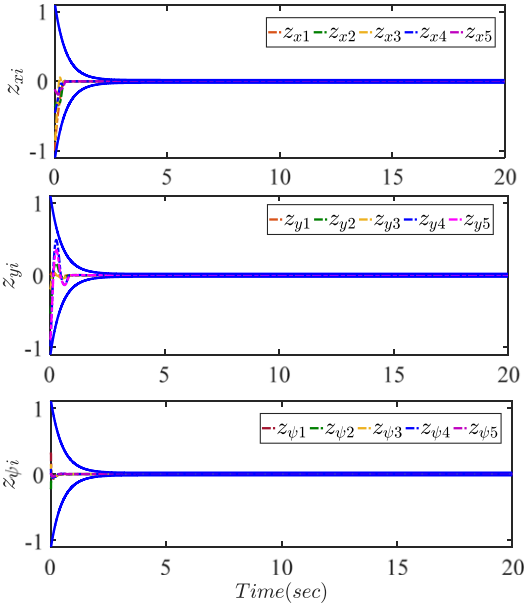

Figure 9. *First surface errors of the autonomous surface vessels* z_{xi}, z_{yi} *and* $z_{\psi i}$.

these approaches, the following performance indices are defined:

$$\begin{cases} ISE = \int_0^T e_i^2(t)dt, \\ IAE = \int_0^T |e_i(t)|\, dt, \\ ITAE = \int_0^T t|e_i(t)|\, dt, \end{cases} \tag{72}$$

https://doi.org/10.1017/S0263574722001266 Published online by Cambridge University Press

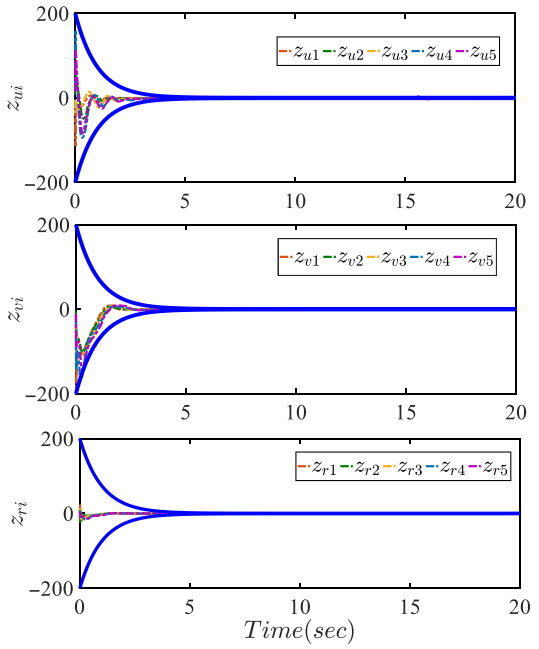

Figure 10. *Second surface errors of the autonomous surface vessels z_{ui}, z_{vi} and z_{ri}.*

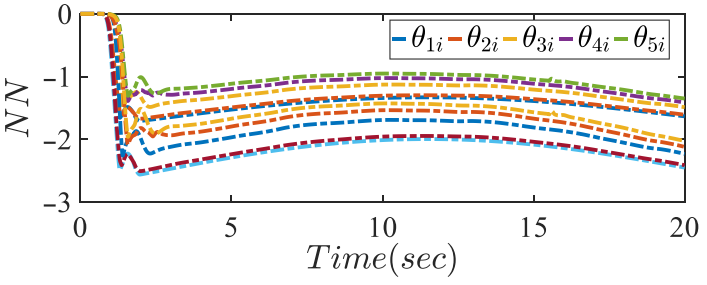

Figure 11. *Frobinious norm of the RBF neural network θ_{1i}, θ_{2i}, θ_{3i}, θ_{4i} and θ_{5i}.*

where $e_i(t)$ is the tracking error of the formation control, T is the constant time in which the transient response settles and Integral Square Error (ISE), Integral Absolute Error (IAE) and Integral Time Absolute Error (ITAE) are the ISE, IAE and ITAE, respectively. The overshoot, settling time, the tracking errors z_{xi}, z_{yi} and $z_{\psi i}$ in terms of three well-known criteria including ISE, IAE and ITAE are reported in Tables I and II, respectively, between four scenarios without considering disturbances and with applying disturbances. Environmental disturbances as currents and waves effects cause the desired performance not to be achieved and the tracking errors of the formation control are transgressed. The forced external disturbances to each autonomous surface vessel are considered as follows:

$$\tau_{di} = \begin{cases} \tau_{d1} = 5\sin(2t) + 5\cos(t), \\ \tau_{d2} = 5\cos(3t) + 5\cos(2t), \\ \tau_{d3} = 5\sin(2t) + 5\sin(t), \end{cases} \tag{73}$$

By a comparison between different scenarios, in Scenario 1, the control structure only assures the tracking of all ASVs without any novelty. In Scenario 2, the BLF approach decreases the formation

https://doi.org/10.1017/S0263574722001266 Published online by Cambridge University Press

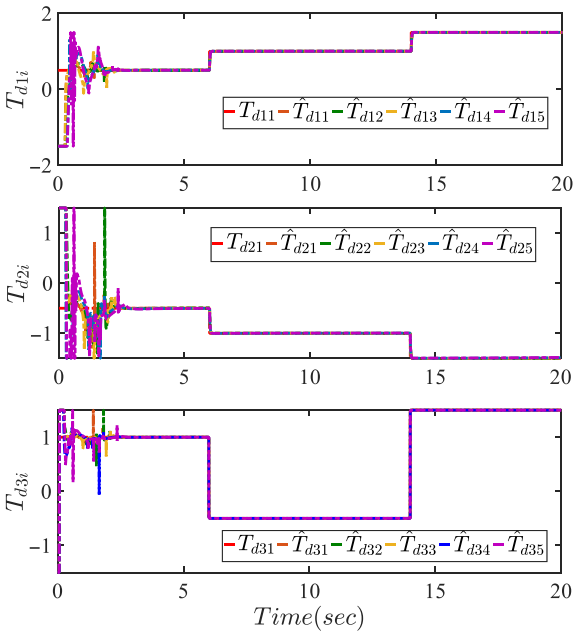

Figure 12. *Disturbance observer output of the autonomous surface vessels τ_{d1i}, τ_{d2i} and τ_{di3}.*

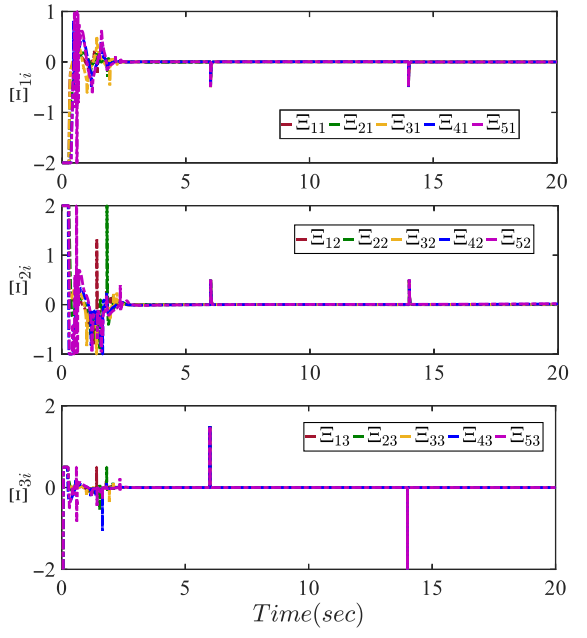

Figure 13. *Disturbance observer errors of the autonomous surface vessels Ξ_{d1i}, Ξ_{d2i} and Ξ_{di3}.*

tracking errors for all ASVs in the defined and limited bounds. In Scenario 3, the finite-time approach decreases the settling time and increases the convergence rate in an effective way. In Scenario 4, the control performance is significantly increased via a combination of the finite-time control and BLF-based design in the control structure. In Fig. 4, the yaw moment τ_r is presented to be much more noisy

https://doi.org/10.1017/S0263574722001266 Published online by Cambridge University Press

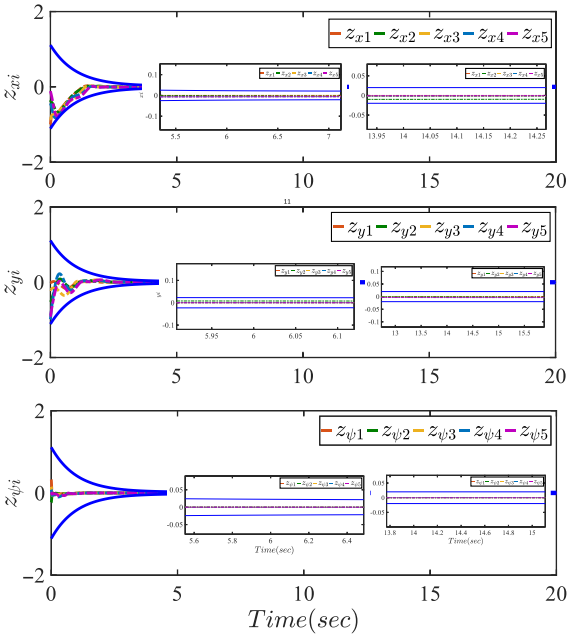

Figure 14. *First surface errors of the autonomous surface vessels z_{xi}, z_{yi} and $z_{\psi i}$ in the presence of imposed external disturbances.*

than τ_u and τ_v. This is because the relative effect of the noise in the yaw dynamics is larger than that one in the surge motion.

5.2. The efficacy and robustness of the proposed controller

To verify the efficacy and robustness of this proposed controller, the following disturbances are applied to the dynamic models of ASVs:

$$\tau_{di} = \begin{cases} \tau_{d1} = +\frac{1}{2}u(t) + \frac{1}{2}u(t-6) + \frac{1}{2}u(t-14) \\ \tau_{d2} = -\frac{1}{2}u(t) - \frac{1}{2}u(t-6) - \frac{1}{2}u(t-14). \\ \tau_{d3} = +1u(t) - 2u(t-6) - \frac{5}{2}u(t-14) \end{cases} \tag{74}$$

As can be seen from Figs. 12 and 13, despite the imposed disturbances to the ASVs dynamics, the desired trajectory tracking of ASVs in the formation control problem is performed well. Although this methodology is an effective approach to handle these disturbances, unwanted peaks are appeared in the disturbance observer errors, while the consecutive step disturbances in Eq. (74) are applied to the ASVs dynamics. In spite of such a peaking, which may be removed by employing the saturation function in the disturbance observer design, all ASVs successfully track the desired trajectories in the formation control problem and the boundary of tracking errors are never transgressed. Moreover, we can see that the finite-time terminal sliding-mode disturbance observer estimates the disturbance τ_{di} quite well for a finite-time presentation of t_{ix}.

It is clear that from Fig. 14, in spite of peaking at $t = 6$ and $t = 8$ s due to the consecutive step disturbances calculated from Eq. (74), all the vehicles construct the desired formation very well. In comparison with the other disturbance observers in the literature, the proposed approach is illustrated as a suitable solution to the problem of disturbance observer design with the finite-time convergence t_{ix}.

https://doi.org/10.1017/S0263574722001266 Published online by Cambridge University Press

Table I. *Comparison results between four scenarios without disturbance effects on ASVs.*

Notation	Overshoot	Settling time	z_x	z_y	z_ψ	ISE	IAE	ITAE
Scenario 1	0.5	2.1	0.19	0.25	0.080	0.009	0.006	0.003
Scenario 2	0.1	1.7	0.13	0.16	0.070	0.008	0.005	0.002
Scenario 3	0.3	0.8	0.20	0.20	0.007	0.008	0.006	0.002
Scenario 4	0.1	1.1	0.13	0.16	0.007	0.007	0.005	0.002

Table II. *Comparison results between four scenarios with disturbance effects on ASVs.*

Notation	Overshoot	Settling time	z_x	z_y	z_ψ	ISE	IAE	ITAE
Scenario 1	0.6	2.9	0.29	0.38	0.09	0.018	0.06	0.009
Scenario 2	0.1	1.9	0.18	0.19	0.08	0.017	0.05	0.008
Scenario 3	0.4	1.6	0.23	0.26	0.008	0.017	0.05	0.009
Scenario 4	0.2	1.9	0.17	0.29	0.008	0.016	0.05	0.008

Moreover, the proposed methodology can eliminate the well-known assumptions on the existence of the derivative of external disturbances in previous works. It is clear that this method does not require any knowledge about the amplitude and frequency of imposed environmental disturbances, and such parameters are not implemented in the controller design.

6. Conclusion

A constrained formation control scheme for a cooperation of autonomous surface vessels was presented in this article. A dynamic surface controller was designed based on the finite-time technique and the reference trajectory of the formation control could be tracked in a finite-time. The formation control of surface vessels employed an adaptive NN technique to compensate the uncertain parameters and unmodeled dynamics. A symmetric BLF was applied to prevent the transgression of the output constraints, and it was illustrated that such outputs are able to start from anywhere in the initial constrained output space. The finite-time BLF-based DSC approach has been combined with a finite-time terminal sliding-mode disturbance observer due to the powerful disturbance rejection of the finite-time technique which increases effectively the convergence rate of the system response and compensates disturbance effects in a finite-time. The obtained simulation results have indicated that the constraints on the formation tracking errors are never violated. Consequently, the formation tracking errors in this newly proposed control algorithm has remained strictly within the constrained region at the finite-time, and the semi-global uniform ultimate boundedness of tracking errors was achieved, and all the closed-loop control signals have remained bounded in the limited and predefined bounds subjected to a mild requirement on the initial conditions.

Authors' contributions.

- Amir Naderolasli: Conceptualization, Investigation, Methodology, Modeling, Design, Simulation, Writing, Editing.
- Khoshnam Shojaei: Conceptualization, Investigation, Methodology, Reviewing, Editing.
- Abbas Chatraei: Methodology, Reviewing, Editing.

Financial support. This research received no specific grant from any funding agency, commercial or not-for-profit sectors.

Conflict of interest. The authors declare none.

Ethical considerations. None.

https://doi.org/10.1017/S0263574722001266 Published online by Cambridge University Press

References

[1] Y. Toda and N. Kubota, "Self-localization based on multiresolution map for remote control of multiple mobile robots," *IEEE Trans. Ind. Inform.* **9**(3), 1772–1781 (2013).

[2] B. M. Yousuf, A. S. Khan and A. Noor, "Multi-agent tracking of non-holonomic mobile robots via non-singular terminal sliding mode control," *Robotica* **38**(11), 1984–2000 (2020).

[3] Y. Dai and S. G. Lee, "Leader–follower formation control of underactuated autonomous underwater vehicles," *Int. J. Control Autom.* **10**(2), 350–361 (2012).

[4] M. N. Huda, H. Yu and S. Cang, "Behavior-based control approach for the trajectory tracking of an underactuated planar capsule robot," *IET Control Theory Appl.* **9**(2), 163–175 (2014).

[5] D. Nakhaeinia and B. Karasfi, "A behavior-based approach for collision avoidance of mobile robots in unknown and dynamic environments," *J. Intell. Fuzzy Syst.* **24**(2), 299–311 (2013).

[6] W. Ren and R. W. Beard, "Formation feedback control for multiple spacecraft via virtual structures," *IEE Proc. Control Theory Appl.* **151**(3), 357–368 (2004).

[7] Y. H. Lee, S. G. Kim, T. Y. Park, S. H. Ji, Y. S. Moon and Y. J. Cho, "Virtual target tracking of mobile robot and its application to formation control," *Int. J. Control Autom. Syst.* **12**(2), 390–398 (2014).

[8] Z. Peng, G. Wen, A. Rahmani and Y. Yu, "Leader–follower formation control of nonholonomic mobile robots based on a bioinspired neurodynamic based approach," *Robot. Auton. Syst.* **61**(9), 988–996 (2013).

[9] K. Shojaei, "Neural network formation control of a team of tractor–trailer systems," *Robotica* **36**(1), 39–56 (2018).

[10] K. Shojaei, "Neural adaptive PID formation control of car-like mobile robots without velocity measurements," *Adv. Robot.* **31**(18), 947–964 (2017).

[11] K. Shojaei, "Neural network formation control of underactuated autonomous underwater vehicles with saturating actuators," *Neurocomputing* **194**(6), 372–384 (2016).

[12] Z. Peng, D. Wang, Z. Chen, X. Hu and W. Lan, "Adaptive dynamic surface control for formations of autonomous surface vehicles with uncertain dynamics," *IEEE Trans. Control Syst. Technol.* **21**(2), 513–520 (2012).

[13] S. L. Dai, S. He, H. Lin and C. Wang, "Platoon formation control with prescribed performance guarantees for USVs," *IEEE Trans. Ind. Electron.* **65**(5), 4237–4246 (2017).

[14] C. Wei, J. Luo, H. Dai and G. Duan, "Learning-based adaptive attitude control of spacecraft formation with guaranteed prescribed performance," *IEEE Trans. Cybern.* **99**, 1–13 (2018).

[15] B. Niu and J. Zhao, "Barrier lyapunov functions for the output tracking control of constrained nonlinear switched systems," *Syst. Control Lett.* **62**(10), 963–971 (2013).

[16] K. P. Tee and S. S. Ge, "Control of nonlinear systems with partial state constraints using a barrier lyapunov function," *Int. J. Control* **84**(12), 2008–2023 (2011).

[17] W. B. Dunbar and R. M. Murray, "Distributed receding horizon control for multi-vehicle formation stabilization," *Automatica* **42**(4), 549–558 (2006).

[18] X. Jin, "Fault tolerant finite-time leader–follower formation control for autonomous surface vessels with LOS range and angle constraints," *Automatica* **68**(2), 228–236 (2016).

[19] W. He, Z. Yin and C. Sun, "Adaptive neural network control of a marine vessel with constraints using the asymmetric barrier lyapunov function," *IEEE Trans. Cybern.* **47**(7), 1641–1651 (2016).

[20] C. Zhang, Y. Yan, A. Narayan and H. Yu, "Practically oriented finite-time control design and implementation: application to a series elastic actuator," *IEEE Trans. Ind. Electron.* **65**(5), 4166–4176 (2017).

[21] C. Zhang, Y. Yan, A. Narayan and H. Yu, "Neural network disturbance observer-based distributed finite-time formation tracking control for multiple unmanned helicopters," *ISA Trans.* **73**(7), 208–226 (2018).

[22] C. Huang, X. Zhang and G. Zhang, "Improved decentralized finite-time formation control of underactuated USVs via a novel disturbance observer," *Ocean Eng.* **174**, 117–124 (2019).

[23] M. Homayounzade and A. Khademhosseini, "Disturbance observer-based trajectory following control of robot manipulators," *Int. J. Control Autom.* **17**(1), 203–211 (2019).

[24] A. Zou, A. H. de Ruiter and K. D. Kumar, "Disturbance observer-based attitude control for spacecraft with input MRS," *IEEE Trans. Aerosp. Electron. Syst.* **55**(1), 384–396 (2018).

[25] A. Mohammadi, M. Tavakoli, H. J. Marquez and F. Hashemzadeh, "Nonlinear disturbance observer design for robotic manipulators," *Control Eng. Pract.* **21**(3), 253–267 (2013).

[26] K. D. Do and J. Pan, "Nonlinear control of an active heave compensation system," *Ocean Eng.* **35**(5), 558–571 (2008).

[27] B. S. Park and J. Pan, "Adaptive formation control of underactuated autonomous underwater vehicles," *Ocean Eng.* **96**(5), 1–7 (2015).

[28] J. Zhang, X. Liu, Y. Xia, Z. Zuo and Y. Wang, "Disturbance observer-based integral sliding-mode control for systems with mismatched disturbances," *IEEE Trans. Ind. Electron.* **63**(11), 7040–7048 (2016).

[29] Y. Zhu, J. Qiao and L. Guo, "Adaptive sliding mode disturbance observer-based composite control with prescribed performance of space manipulators for target capturing," *IEEE Trans. Ind. Electron.* **66**(3), 1973–1983 (2018).

[30] H. Chen, H. Ren, Z. Gao, F. Yu, W. Guan and D. Wang, "Disturbance observer-based finite-time control scheme for dynamic positioning of ships subject to thruster faults," *Int. J. Robust. Nonlin. Cont.* **31**(13), 6255–6271 (2021).

[31] X. Hu, X. Wei, Y. Kao and J. Han, "Robust synchronization for under-actuated vessels based on disturbance observer," *IEEE Trans. Intell. Transp. Syst.* **23**(6), 5470–5479 (2021). doi: 10.1016/j.isatra.2020.12.044

[32] J. Ghommam and A. Chemori, "Adaptive RBFNN finite-time control of normal forms for underactuated mechanical systems," *Nonlinear Dyn.* **90**(1), 301–315 (2017).

https://doi.org/10.1017/S0263574722001266 Published online by Cambridge University Press

[33] C. Huang, X. Zhang and G. Zhang, "Adaptive neural finite-time formation control for multiple underactuated vessels with actuator faults," *Ocean Eng.* **222**, 108556 (2021).
[34] Z. Peng, J. Wang, D. Wang and Q. L. Han, "An overview of recent advances in coordinated control of multiple autonomous surface vehicles," *IEEE Trans. Ind. Inform.* **17**(2), 732–745 (2020).
[35] N. Gu, D. Wang, Z. Peng, J. Wang and Q. L. Han, "Advances in line-of-sight guidance for path following of autonomous marine vehicles: an overview," *IEEE Trans. Syst. Man Cybern. Syst.*, 1–17 (2022). https://ieeexplore.ieee.org/document/9750396
[36] N. Gu, D. Wang, Z. Peng, J. Wang and Q. L. Han, "Disturbance observers and extended state observers for marine vehicles: A survey" control eng," *Cont. Eng. Pract.* **123**, 105158 (2022).
[37] J. Yu, X. Dong, Q. Li, J. Lu and Z. Ren, "Adaptive practical optimal time-varying formation tracking control for disturbed High-Order Multi-Agent systems," *IEEE Trans. Circ. Syst. I* **69**(6), 2567–2578 (2022). doi: 10.1109/TCSI.2022.3151464.
[38] H. Du, W. Zhu, G. Wen, Z. Duan and J. Lu, "Distributed formation control of multiple quadrotor aircraft based on nonsmooth consensus algorithms," *IEEE Trans. Cybern.* **49**(1), 342–353 (2017).
[39] W. Ren, "Consensus Tracking Under Directed Interaction Topologies: Algorithms and Experiments," **In:** *2008 American Control Conference* (IEEE, June 2008) pp. 742–747.
[40] N. Gu, D. Wang, Z. Peng and J. Wang, "Safety-critical containment maneuvering of underactuated autonomous surface vehicles based on neurodynamic optimization with control barrier functions," *IEEE Trans. Neur. Net. Lear.,* 1-14 (2021). doi: 10.1109/TNNLS.2021.3110014.
[41] K. P. Tee, B. Ren and S. S, "Ge "Control of nonlinear systems with time-varying output constraints," *Automatica* **47**(11), 2511–2516 (2011).
[42] K. P. Tee, S. S. Ge and E. H. Tay, "Barrier Lyapunov functions for the control of output-constrained nonlinear systems," *Automatica* **45**(4), 918–927 (2009).
[43] B. Xiao, X. Yang and X. Huo, "A novel disturbance estimation scheme for formation control of ocean surface vessels," *IEEE Trans. Ind. Electron.* **64**(6), 4994–5003 (2016).
[44] N. Sarrafan and K. Shojaei, "High-gain observer-based neural adaptive feedback linearizing control of a team of wheeled mobile robots," *Robotica* **38**(1), 69–87 (2020).
[45] K. P. Tee and S. S. Ge, "Control of fully actuated ocean surface vessels using a class of feedforward approximators," *IEEE Trans. Contr. Syst. Trans.* **14**(4), 750–756 (2006).
[46] H. K. Khalil, "Cascade high-gain observers in output feedback control," *Automatica* **80**, 110–118 (2017).

Cite this article: A. Naderolasli, K. Shojaei and A. Chatraei (2023). "Terminal sliding-mode disturbance observer-based finite-time adaptive-neural formation control of autonomous surface vessels under output constraints", Robotica **41**, 236–258. https://doi.org/10.1017/S0263574722001266